Seismic Waves from Light Trucks Moving Over Terrain

Stephen A. Ketcham, Mark L. Moran, and James Lacombe
USACE Engineer Research and Development Center, Cold Regions Research and Engineering Laboratory (ERDC-CRREL), Hanover, NH
{Stephen.A.Ketcham, Mark.L.Moran, James.Lacombe}@erdc.usace.army.mil

Abstract

Seismic sensing is one sensor mode employed in US unattended ground sensor systems (UGS). Seismic sensors possess the advantage of beyond-line-of-sight sensing. They can detect ground vibrations generated by moving vehicles or personnel, and they can be used to cue other sensors or possibly to classify or even identify targets. As a complement to field trials, our work has produced a simulation capability to support seismic UGS developments. We model ground vibrations from moving vehicles and generate synthetic seismic wavefield data over terrain of interest to US forces. Using supercomputers to simulate seismic wave propagation in large finite-difference time-domain simulations, our objective is to generate high fidelity data sets that provide new opportunities for understanding and exploiting signal features that may be unrecognizable in limited field trials. The method utilizes a vehicle-dynamics model to calculate the vehicle response to vehicle acceleration and movement over bumpy roads or terrain. It calculates forces transmitted to the ground; distributes these forces to grid points of a finite difference model; and simulates seismic waves propagating away from the vehicle. The current work focuses on light trucks moving toward and through a mountain pass and signature features associated with suspension and wheelbase characteristics. The results from two analyses show seismic waves propagating away from one and two trucks, respectively. We conclude that the wavefield data is realistic and suitable for virtual trials of seismic UGS.

1. Introduction

> *"The mission was to cut off a major supply route, call attention to the Marines' presence, and impede those fleeing as Kandahar fell to Anti-Taliban freedom fighters. A major road, tagged Route 1, was chosen and the Marines positioned themselves to intercept Taliban running from the fierce fighting in the city.*
>
> *Two platoons of HMMWVs mounted with TOW missile systems, automatic grenade launchers, and .50-caliber machine guns pushed east and west to monitor traffic exiting the two cities of interest. One watched for bad guys coming out of Kandahar to the east and the other reported those leaving Lashkar Gah. Reports of a Sports Utility Vehicle heading from Kandahar warmed the chilly night....*
>
> *...Another report came over the radio as the Marines began their retrograde. The SUV just destroyed turned out to be leading a seven-vehicle convoy."* (Chenelly, 2002)

In recent conflicts, the US military has often encountered light trucks operated by threat forces. US ground forces, base camps, and other interests have been attacked by pickup trucks advancing rapidly over rugged terrain, and US forces have engaged threat sport utility vehicles singly and in convoys. While US unattended ground sensor systems (UGS) include methods to detect, track, and classify vehicles, this remains a difficult problem in practice. It is difficult, for example, for an UGS to track multiple vehicles or to distinguish a light truck as a threat vehicle. Research is ongoing to mitigate these deficiencies.

Seismic sensing is one sensor mode employed in multimode UGS. Like acoustic sensors, they possess the advantage of beyond-line-of-sight sensing. Seismic sensors can detect ground vibrations generated by moving vehicles or personnel, and they can be used to cue other sensors or to classify and even identify targets. The success of seismic sensing depends on the range to a vibration source and the complicating effects of subsurface geology and topography. If a seismic sensor can adapt to local geologic conditions, or be employed at an optimal location, it will produce better information for vehicle tracking and signature analysis.

To date, field measurements have been the bases of most advances in seismic vehicle sensing. As a complement to field trials, our work has produced a high-fidelity simulation capability to support seismic UGS developments. We model ground vibrations from moving vehicles and generate synthetic seismic wavefield data over terrain of interest to US forces. Using supercomputers to analyze large detailed models, we have new opportunities for understanding and exploiting signal features that may be unrecognizable in limited field trials.

We simulate seismic wave propagation in large finite-difference time-domain (FDTD) simulations. The computations realistically produce ground vibrations from moving vehicles across a bandwidth of interest. We model lower frequency loading associated with suspension dynamics up to higher frequency impulsive loading associated with tire treads of wheeled vehicles or track blocks of tracked vehicles. The method utilizes a vehicle-dynamics model to calculate the vehicle response to vehicle acceleration and movement over bumpy roads or terrain. It calculates forces transmitted to the ground; distributes these forces to grid points of a finite difference model; and simulates seismic waves propagating away from the vehicle.

The current work focuses on light trucks moving toward and through a mountain pass and signature features associated with suspension and wheelbase characteristics. We present the results from two FDTD analyses that show seismic waves propagating away from one and two trucks, respectively. The paper describes the vehicle and geologic models used in the analyses, the vehicle solutions that produce the force inputs to the FDTD models, and the seismic propagation analyses. We demonstrate and conclude that the wavefield data is realistic and suitable for virtual trials of seismic UGS.

2. Vehicle and Geologic Models

For results in this paper, we use a geologic model having the surface topography of a 2 km by 2 km area around Oliverian Notch in the New Hampshire White Mountains. Figure 1 illustrates the topographic surface, which derives from a 10-m-resolution digital elevation map of the USGS Warren, New Hampshire Quadrangle. Oliverian Notch is a mountain gap through which New Hampshire Highway 25 passes.

The subsurface is a synthesized geology consisting of bedrock and a valley of soil that extends to a depth of approximately 25 m. Figure 2 depicts the depth to bedrock over the model extents.

Table 1 presents the seismic properties that model the bedrock and soil of the geologic model. These are the compression- and shear-wave speeds, the densities, and the material attenuation factors for compression and shear waves.

Table 1. Material constants of geologic model

Material	Compression wave speed (m/s)	Shear wave speed (m/s)	Density (kg/m3)	Material attenuation factor for compression waves	Material attenuation factor for shear waves
Soil	1000	577	1750	25	9
Bedrock	3000	2000	2400	150	67

The vehicle model is a bounce and pitch model (e.g., Gillespie, 1992). The assigned properties, listed in Table 2, define two "generic" light trucks for the FDTD analyses. These are meant to represent a light-truck lightly loaded (LT#1) and the same truck heavily loaded (LT#2). The models bounce and pitch in response to the roughness of the terrain or road over which they travel and in response to their forward acceleration.

Our preprocessing assigns the forces in the vehicle springs/dashpots to model nodes at the four wheel locations to simulate continuous vehicle movement over the model surface. Ketcham et al. (2004) describes the vehicle model and the preprocessing of the force data for input to the FDTD calculations.

Table 2. Model constants for light trucks[c]

Vehicle	Mass (kg)	Moment of inertia (kg m^2)	Wheelbase (m)	Spring stiffness (kN/m)[a]		Damping constant (kNs/m)[b]		Height of center of mass (m)
				Front	Rear	Front	Rear	
LT#1	2000.	700.	2.8	70.	90.	2.3	3.0	0.75
LT#2	2800.	700.	2.8	70.	90.	2.3	2.0	0.75

[a] Two sets of the springs model both left and right wheel springs. Track width is 1.7 m.

[b] The damping constants are proportional to the stiffness values. The damping models each vehicle's shock absorbers.

[c] The uncoupled damped natural frequencies are 1.40 Hz and 3.13 Hz for the LT#1 bounce and pitch modes, respectively; the LT#1 uncoupled damping ratios are 0.15 and 0.35, respectively. For LT#2, the natural frequencies are 1.17 Hz and 3.44 Hz. The uncoupled damping ratios are 0.15 and 0.43.

3. Vehicle Paths, Accelerations, and Solutions

We processed vehicle inputs for two FDTD analyses. The first analysis used force inputs from the vehicle LT#1 moving over the path illustrated in Figure 3. This path roughly followed the approach and transit of Highway 25 through Oliverian Notch. The second analysis repeated the LT#1 inputs and added ground forcing from the vehicle LT#2 moving over part of the LT#1 path, but at a lower speed. Figure 4 illustrates the LT#2 path. For both analyses, we superimposed the roughness of a gravel

highway (Gillespie, 1992) on the topographic surface to excite vehicle vibrations in a realistic manner.

Figures 5 and 6 illustrate the vehicle dynamics solutions from which the input forces to the seismic analyses derive. The path elevations in these figures reveal that the vehicle LT#1 began its drive before the rise to the highest path elevation, whereas LT#2 began its drive near the highest path elevation. In addition, the LT#1 vehicle acceleration reached noticeably higher values than LT#2. The intent of the simulation was that the lightly loaded LT#1 was able to move at a higher speed along the gravel road, whereas the heavily loaded LT#2 could only lumber along. The two different vehicle bounce-and-pitch responses reveal differences attributable to the different vehicle rides.

From the bounce and pitch solutions, the spring and dashpot forces were calculated and distributed to nodes along the vehicle paths. We saved data files of the force distributions in space and time for subsequent input to the finite difference analysis. Figures 7 and 8 present a check of the saved data for vehicle LT#1. In Figure 7, the summed forces of the vehicle dynamics solution match the summed forces of the distributed force inputs, as they should. In Figure 8, the force applied to a single node shows the realistic variation of force as front then rear wheels travel near to the node. We observed similar results for vehicle LT#2.

4. Seismic Propagation Analyses

The method used for the seismic analysis is a variable grid seismic FDTD method that allows a ground to air interface at the topographic surface in order to model the free surface boundary condition. The variable grid provides for more accurate modeling in the presence of the "staircased" topography. It also allows for more efficient modeling, as the grid can expand greatly from the soil to the bedrock (by a factor of 9 vertically in the current model) while still maintaining sufficient nodes per minimum wavelength for accuracy. The elastic formulation and its accuracy are detailed in Ketcham and Moran (2004). We apply viscoelasticity to simulate material attenuation according to Robertsson et al. (1994).

The two analyses performed for the current work were designated on 7_SUV1 and on 7_SUV2. As mentioned, the first analysis is of vehicle LT#1 moving over the path in Figure 3. The second analysis repeats this vehicle path and adds LT#2 moving over the path in Figure 4, resulting in two vehicles moving over the same roadway.

The FDTD code is written in FORTRAN. It operates on rectangular sub domains and uses MPI to pass information between domains. The code is vectorized for use on the Cray X1. Both analyses ran on the ERDC MSRC X1, using 40 multiprocessors. The number of nodes for the geologic model was 118.8e6. The number of time steps was 225050. The wall time of the second, more demanding computation was 15.3 h.

Results of analysis on 7_SUV1 are in Figures 9 and 10. Figure 9 presents a sequence of vertical particle velocity wavefields on the surface of the model, while Figure 10 presents analysis of the particle velocity data from a single sensor location. Figures 11 and 12 present the corresponding results for analysis on 7_SUV2.

5. Discussion of Analyses and Results

The wavefields of the two analyses show succeeding locations of the vehicles and the complexity of the surface waves that emanate from the vehicles. From the first analysis, the Figure 9 results show higher amplitude and more-complicated waveforms in the areas where the soil is present. The soil valley acts to reflect, refract, trap, and channel the seismic propagation. Where the bedrock is shallow or at the surface, the waveforms spread out to a longer wavelength with more clarity in their form.

From the second analysis, the Figure 11 results show the LT#1 vehicle starting out behind the LT#2 vehicle, and then catching up and overtaking the slower-moving LT#2. The amplitudes are greater in the second analysis, due to multiple vehicle inputs as well as to the force inputs of the heavier LT#2. The combination of the vehicle inputs also increases the complexity of the waveforms. The vehicles produce distinct but interfering waveforms for much of the analysis, but as LT#1 comes close to LT#2, the waveforms combine to resemble waveforms from a single source.

The spectral displays in Figures 10 and 12 show intermittent energy at the frequency of predictable wheelbase filtering frequencies. Wheelbase filtering is a term given to the effect that the wheelbase, i.e., the distance from front to rear wheels, has on the comfort of a vehicle's ride (Gillespie, 1992). Since a vehicle's front then rear wheels hit a bump in succession, the familiar "bump-bump" occurs at a frequency that is the vehicle speed divided by the wheelbase. For continuous road roughness, this results in seismic energy being emitted at this frequency. The predicted harmonics in Figures 10 and 12 overlie intermittent energy at this speed-dependent frequency, demonstrating that the simulation captures this important signature characteristic when the complicating effects of the geology do not obscure the signature. When evident, the wheelbase-filtering signal follows the variation in vehicle speed, which is also shown in Figures 10 and 12.

In the Figure 12 spectrogram, the predicted wheelbase filtering frequency of only the LT#2 traverse is indicated. Referring back to Figure 10, the observer can

see that the wheelbase filtering frequency of LT#1 also reveals itself occasionally throughout the duration of the Figure 12 spectrogram.

In addition to the signature of the wheelbase filtering, the bounce-mode damped natural frequencies of the vehicles also appear in the spectral energy displays. Unlike the wheelbase filtering, however, this signature characteristic does not depend on the vehicle speed. In particular, the 1.4-Hz bounce-mode frequency of the vehicle LT#1 reveals itself fairly strongly in Figure 10. This may be the case in the second analysis on 7_SUV2, but the bounce mode frequencies of the LT#1 and LT#2 vehicles are different (1.4 and 1.17 Hz, respectively) yet too close to be distinguishable in Figure 12. There is, however, energy evident around the bounce mode frequencies in Figure 12.

6. Conclusions

The results of two seismic simulations of light trucks moving through a mountain pass demonstrate that signature features of moving model vehicles propagate from the vehicles to the remote location of a virtual sensor. One signature feature was independent of the vehicle speed while the other was dependent on the speed. The realistic nature of the simulations makes their data sets candidates for further processing in support of UGS seismic algorithm development, and shows that seismic simulations in complex terrain can supplement cost-limited UGS field trials.

Acknowledgement

Computational resources were provided by the Department of Defense High Performance Computing Modernization Program under DoD Challenge Project C76. This work was supported by the Battlespace Environment Program of the US Army Corps of Engineers, Engineering Research and Development Center.

References

Chenelly, J.R., 15th MEU (SOC) Halts Fleeing Taliban, 15th Marine Expeditionary Unit Story Number 2002111162655, available at http://www.usmc.mil/marinelink/mcn2000.nsf/0/34c7274372bdf01185256b3e0075d226, 2002.

Gillespie, T.D., *Fundamentals of Vehicle Dynamics*, Society of Automotive Engineers, Warrendale, PA, 1992.

Ketcham, S., M. Moran, J. Lacombe, R. Greenfield, and T. Anderson, "Seismic Source Model for Moving Vehicles." Manuscript TGRS-00055-2004 accepted for publication., *IEEE Transactions on Geoscience and Remote Sensing*, 2004.

Ketcham, S., and M. Moran, "Variable-Grid Transformation for FDTD Seismic Simulations." Manuscript for publication, 2004.

Robertsson, J., J. Blanch, and W. Symes, "Viscoelastic Finite-Difference Modeling." *Geophysics*, Vol. 59, 1994, pp. 1444–1456.

Wong, J.Y., *Theory of Ground Vehicles*, Second Edition, John Wiley, New York, 1993.

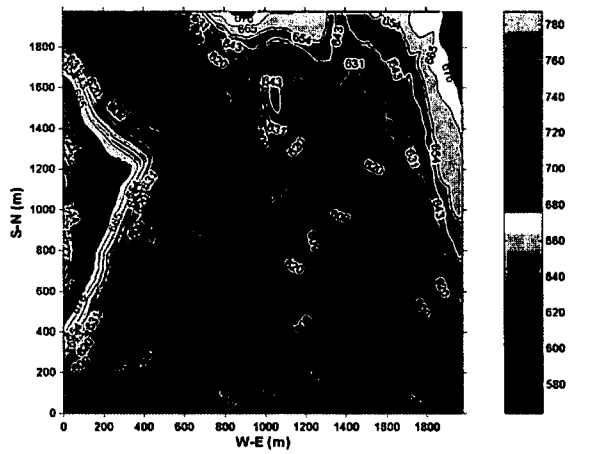

Figure 1. Surface contour graph of geologic model illustrating topography around mountain pass. Contour values and colorbar scale are in meters above an arbitrary datum. The highest elevation is colored lighter gray. The lowest elevation is colored darker green.

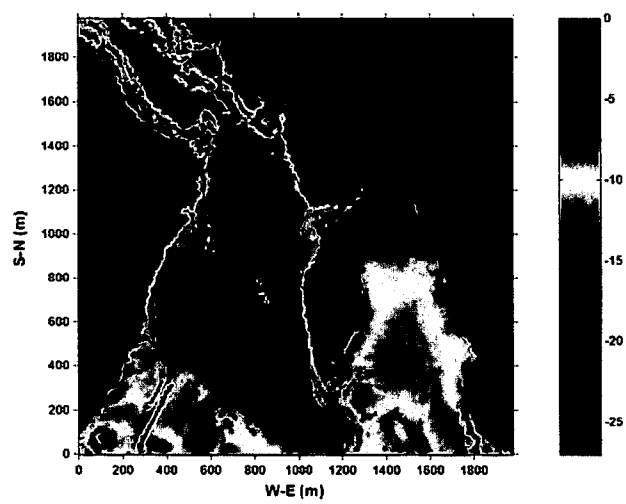

Figure 2. Color graph of geologic model illustrating depth to bedrock from topographic surface. Colorbar scale is the elevation of the bedrock surface in meters relative to the topography in Figure 1. The deeper soil deposits are colored blue. The bedrock is at or near to the surface where the color is deep red.

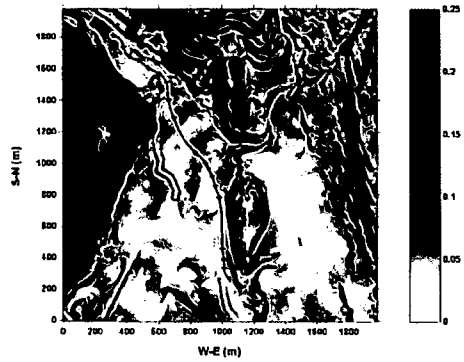

Figure 3. Path of vehicle LT#1 in the first and second seismic propagation analyses, plotted on a color graph illustrating slope of topographic surface. The maximum slope indicated is set to 0.25, although the slope is much greater at some locations on the surface. The path is the blue line, and the direction of travel is south to north. The points used to define the spline-curve path are the red symbols. The path follows gently sloping topography.

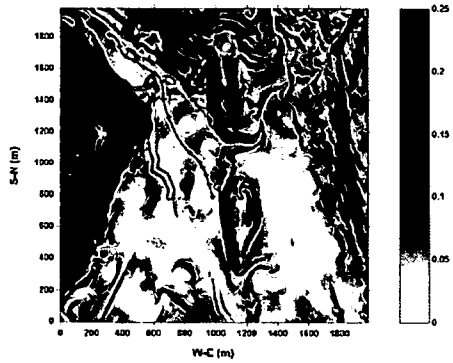

Figure 4. Path of vehicle LT#2 in the second seismic propagation analysis, plotted on the graph of the topographic slope. The path is the blue line. The points used to define the path are the red symbols, which are coincident with the 15 Northern most pick points in Figure 3.

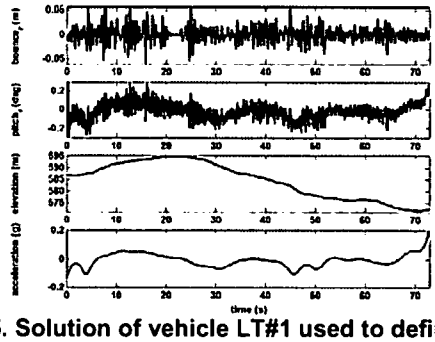

Figure 5. Solution of vehicle LT#1 used to define input forces for the first and second seismic propagation analyses. The two lower graphs show the vehicle acceleration along its path and the gross features of the topographic surface; the vehicle bounces and pitches in response to these excitations as well as to the fine scale roughness of the road. The upper graphs plot the vehicle bounce and pitch relative to the ground surface.

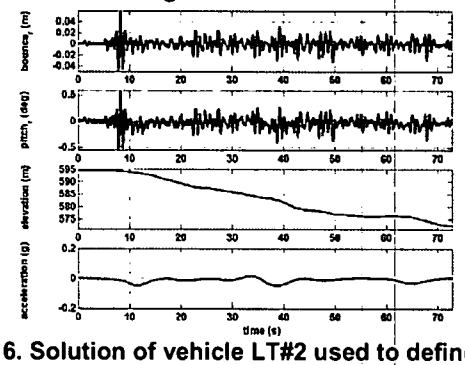

Figure 6. Solution of vehicle LT#2 used to define input forces for the second seismic propagation analysis.

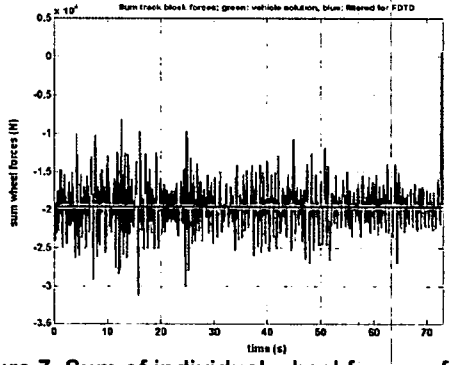

Figure 7. Sum of individual wheel forces of first seismic propagation analysis. The green line shows the summed forces from the vehicle dynamics solution. The blue line, which is hard to distinguish because it coincides with the green line (as it should), shows a summation of the forces distributed to the finite difference surface nodes. The black line is the vehicle weight. As expected, the summed input forces oscillate around the vehicle weight.

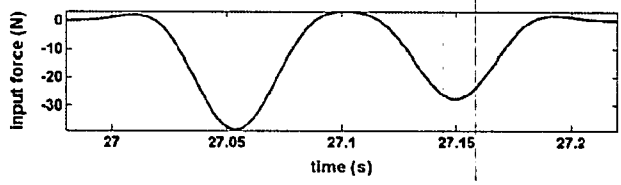

Figure 8. An example of the force applied to a single node in the finite difference analysis as a result of front and rear wheels passing the node in succession. The variation in load is of the form expected for a subsurface location within the pressure distribution of a tire (e.g., Wong, 1993).

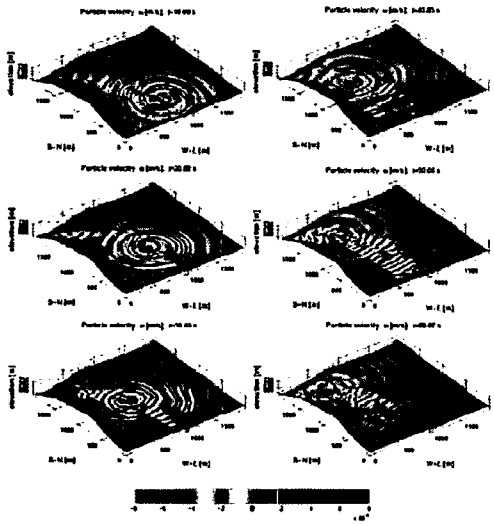

Figure 9. Seismic waves generated by moving vehicle LT#1 in analysis on 7_SUV1. The graphs show images of vertical particle velocity *w* over topographic surface from vehicle forces at times=10, 20, 30, 40, 50, and 60s. The colorbar maps to the particle velocity amplitude. The colorbar maxima were set to +-e^{-8}m/s to optimally highlight the wavefield across the model.

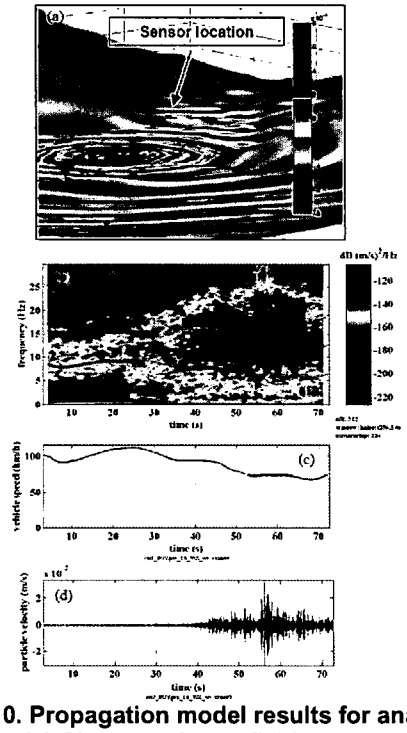

Figure 10. Propagation model results for analysis on 7_SUV1. (a) Closeup of wavefield on model surface and sensor location, which is on the surface at W-E=500 m and S-N=1500 m; (b) Spectrogram of seismic signal showing the evolving spectral character of the seismic signal at the receiver location; (c) Speed vs. time of vehicle LT#1; and (d) Vertical particle velocity at receiver location vs. time. The shaded lines in the spectrogram are three wheelbase filtering harmonics predicted by i × speed/wheelbase, i=1, 2, 3.

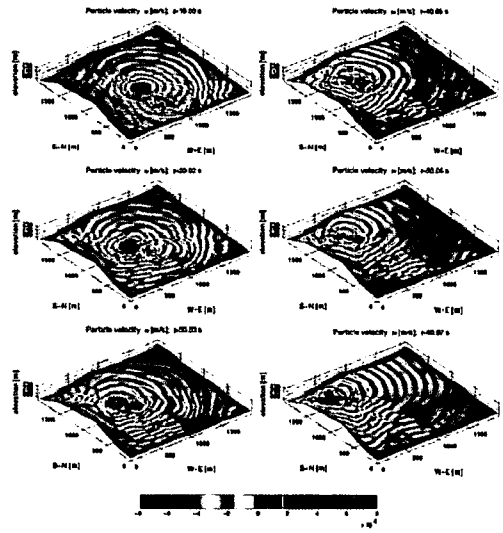

Figure 11. Seismic waves generated by vehicles LT#1 and LT#2 in analysis on 7_SUV2.

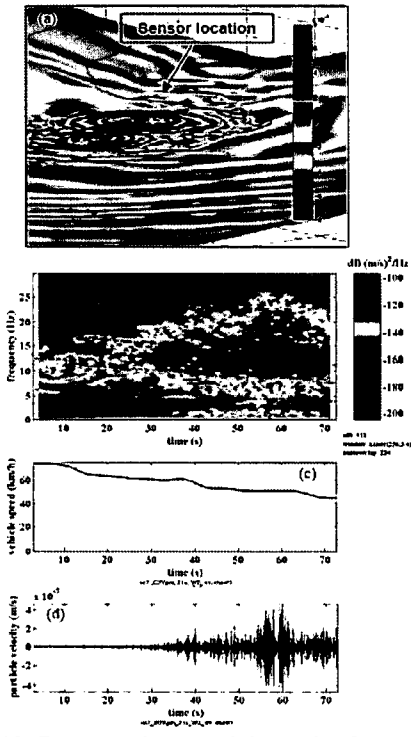

Figure 12. Propagation model results for analysis on 7_SUV2. (a) Closeup of wavefield on model surface and sensor location at W-E=500 m and S-N=1500 m; (b) Spectrogram of seismic signal; (c) Speed vs. time of vehicle LT#2; and (d) Vertical particle velocity at receiver location vs. time. The shaded lines in the spectrogram are three wheelbase filtering harmonics for the vehicle LT#2. The predicted harmonics for LT#1 are not shown.